Articles

NMR Studies of the Interaction of Tryparedoxin with Redox-Inactive Substrate Homologues†

Dirk Krumme,*,‡ Heike Budde,§ Hans-Jürgen Hecht,‡ Ulrich Menge,§ Oliver Ohlenschläger,|| Anton Ross,⊥ Josef Wissing,§ Victor Wray,‡ and Leopold Flohé§

Department of Structural Biology and Research Group Bioreaction Techniques, German Research Centre for Biotechnology, and Department of Biochemistry, University of Braunschweig, Mascheroder Weg 1, D-38124 Braunschweig, Germany, and Department of Molecular Biophysics/NMR-Spectroscopy, Institute for Molecular Biotechnology, Beutenbergstrasse 11, D-07745 Jena, Germany

Received May 6, 2003; Revised Manuscript Received August 5, 2003

ABSTRACT: Tryparedoxins (TXNs) are trypanothione-dependent peroxiredoxin oxidoreductases involved in hydroperoxide detoxification that have been shown to determine virulence in trypanosomatids. The structure of ^{15}N,^{13}C-doubly-labeled, C-terminally-His-tagged tryparedoxin 1 from *Crithidia fasciculata* (*Cf* TXN1) was elucidated by three-dimensional NMR spectroscopy. Global folding was found to be similar to the crystal structure, but regions near the active site, especially the onset of helix α1 with the redox-active Cys 43 and helix α2 relevant to substrate binding, were less well defined in solution. The redox-inactive inhibitory substrate analogue N^1,N^8-bis(ophthalmyl)spermidine was used to study the substrate/TXN interaction by two-dimensional ^1H,^{15}N NMR spectroscopy. The NMR data complemented by molecular modeling revealed several alternative modes of ligand binding. The results confirm and extend the concept of TXN action and specificity derived from X-ray analysis and site-directed mutagenesis and thus improve the rational basis for inhibitor design.

The fight against trypanosomiasis and leishmaniasis has remained one of the great challenges in global health care (*1*). The parasitic trypanosomatids still affect about 40 million people and are estimated to cause 500000 fatalities per year. The efforts to combat the devastating diseases range from control of the insect vectors to vaccination strategies and search for novel drugs (*2*). Antigen variation and mimicry, as is common in this group of parasites, have so far rendered immunological strategies unsuccessful. Available drugs suffer from limited efficiency, unaffordable costs, and substantial toxicity (*3*, *4*).

Metabolic pathways that are unique to, and of vital importance for, these parasites promise a chance to create efficient and safe therapeutics by rational inhibitor design. The trypanothione-dependent hydroperoxide detoxification system of trypanosomatids, which was discovered in the insect pathogen *Crithidia fasciculata* (*5*), appears to meet the criteria of an attractive drug target area: Inverse genetics revealed that the pathway is pivotal to the virulence and viability of *Leishmania donovani* (*6*) and *Trypanosoma brucei* (*7*), and the constituting enzymes trypanothione reductase, tryparedoxin (TXN),[1] and the peroxiredoxin-type tryparedoxin peroxidase (TXNPx) are sufficiently distinct from analogous or homologous mammalian proteins (*8*−*10*).

The focus of this work is on TXN, which is the oxidoreductase that catalyzes the reduction of the terminal peroxidase by trypanothione [N^1,N^8-bis(glutathionyl)spermidine, $T(SH)_2$]. The protein is remotely related to thioredoxin, but 50% larger and characterized by the unusual active site motif WCPPCR. Unlike thioredoxin it is not directly reduced by any of the flavin-containing disulfide reductases but specifically by trypanothione, which uniquely occurs in trypanosomatids (*11*). In view of these peculiarities, detailed insights into the TXN/trypanothione interaction are considered to be instrumental for future inhibitor design. Previous attempts to solve this task by cocrystallization of oxidized TXN with its natural substrate have failed as only reduced TXN with no substrate or product was detected (*12*). Only when a catalytically inactive molecular mutant of *Cf* TXN 2 (*Cf* TXN2C44S) was reacted with the truncated substrate glutathionylspermidine was a dead-end intermediate obtained that

† The work was partially supported by the Deutsche Forschungs Gemeinschaft (Grant Fl 61/11-3).

* To whom correspondence should be addressed. Phone: +49(0)-531-6181-372. Fax: +49(0)531-6181-355. E-mail: hjh@gbf.de.

‡ Department of Structural Biology, German Research Centre for Biotechnology.

§ University of Braunschweig.

|| Institute for Molecular Biotechnology.

⊥ Research Group Bioreaction Techniques, German Research Centre for Biotechnology.

[1] Abbreviations: TXN, tryparedoxin; *Cf*, *Crithidia fasciculata*; *Tb*, *Trypanosoma brucei*; $T(SH)_2$, trypanothione [N^1,N^8-bis(glutathionyl)-spermidine]; BOS, N^1,N^8-bis(γ-Glu-Ala-Gly)spermidine, N^1,N^8-bis-(ophthalmyl)spermidine; FID, free induction decay.

10.1021/bi030112d CCC: $25.00
Published on Web 11/26/2003

was stable enough to be crystallized. On the basis of pertinent X-ray data, a model of the TXN/T(SH_2) interaction was developed that, however, had to rely in many aspects on circumstantial evidence inferred from site-directed mutagenesis (*12*). Complementary information on the TXN/substrate interaction could be expected by studying binding of the substrate mimic N^1,N^8-bis(ophthalmyl)spermidine (BOS), which differs from T(SH_2) in having the redox-active cysteines replaced by alanines. Unexpectedly, BOS did not cocrystallize with TXN. Hence, we have elucidated the 3-D structure of TXN in solution by NMR techniques and studied its interaction with BOS using pseudosubstrate-induced chemical shift data.

EXPERIMENTAL PROCEDURES

Production and Purification of ^{15}N,^{13}C-Labeled Cf TXN1. Recombinant C-terminally-His-tagged TXN1 from *Cf* (*Cf* TXN1) was heterologously expressed in *E. coli* strain BL21-(DE3)pLys transformed with the plasmid pET22b(+)/TXN1H6 (*13*) and cultivated in a medium having NH_3 and glucose replaced by [^{15}N]NH_3 and [^{13}C]glucose (Cambridge Isotope Laboratories Inc., Andover, MA) with >98% isotope purity. The His-tagged ^{15}N,^{13}C-*Cf* TXN1 was purified by metal affinity chromatography. Its sequence corresponds to that of wild-type *Cf* TXN1 (accession no. AF 084456) with the exception that a leucine, a glutamine, and six histidine residues are added to the C-terminus. The specific activity of the preparation (59.7 U/mg) complied with that of unlabeled ones (*13*). The isotope purity of the protein was verified by MALDI-TOF analysis of tryptic peptides to be >98%. The preparation was concentrated to give samples suitable for NMR (1 mM protein in 1 mM aqueous potassium phosphate, pH 6.5, with 0.02% NaN_3 and 10% D_2O).

S*ynthesis of the Pseudosubstrate.* N^1,N^8-Bis(γ-Glu-Ala-Gly)spermidine [N^1,N^8-bis(ophthalmyl)spermidine, BOS] was synthesized by successive addition of amino acids to an N^4-Z-protected spermidine. Addition of the residues was performed by aminolysis of the appropriate Boc-protected *N*-succinyl esters. Boc groups were removed by aqueous HCl in 2,2,2-trifluoroethanol. After evaporation the products were obtained as hydrochlorides. Aminolysis of Boc-Glu(OSu)-O^{t}Bu by N^1,N^8-bis(H-Ala-Gly)spermidine-N^4-Z gave the protected BOS derivative, which was purified by chromatography on Sephadex LH20 with methanol. Total deprotection was carried out either by acidolysis with HBr/acetic acid (*14*) or by hydrogenolysis of the Z group with H_2/Pd in methanol and following hydrolysis with aqueous HCl/trifluoroethanol. The product and intermediates were identified by NMR spectroscopy and mass spectrometry. Analoguous compounds with central diamines instead of spermidine were synthesized accordingly.

Enzyme Assays. TXN activity was monitored by NADPH consumption in a reconstituted trypanothione peroxidase system according to Flohé et al. (*15*). For inhibition studies, the assay was performed in a 500 μL reaction volume containing 10 μM TXN peroxidase (*Cf* H6TXNPx), 225 μM NADPH (Sigma, Steinheim, Germany), 1 U/mL trypanothione reductase, and 10 μM *Cf* TXN2H6, *Cf* TXN1H6, or *Tb* TXN in 50 mM Tris−HCl, 1 mM EDTA, pH 7.6, T($SH)_2$ (Bachem, Heidelberg, Germany) in concentrations of 0.6−1.3 μM, and the pseudosubstrate in a range from 400 to 1500 μM. The mixture was preincubated for 15 min at 25 °C, and the reaction was started by adding 70 μM *tert*-butyl hydroperoxide.

NMR Spectroscopy and Structure Calculation. Heteronuclear NMR spectra were recorded at 600 MHz on a Bruker Avance DMX 600 and at 750 MHz on a Varian Unity INOVA 750 narrow-bore NMR spectrometer at 30 °C. Bruker spectra were acquired using XWIN-NMR 1.3 (Bruker, Rheinstetten, Germany) software. Processing of the raw data was carried out with XWIN-NMR 1.3 or 3.0. Triple-resonance spectra were processed using zero filling and linear prediction to give 1K data points in the direct ^1H dimension and 512 and 128 data points in the ^{13}C and ^{15}N dimensions, respectively. FIDs obtained from the Varian spectrometer were converted and processed with XWIN-NMR 3.0 to yield spectra with 1K data points in the direct ^1H dimension and 512 data points in the indirect dimensions. Analysis of the processed spectra including peak picking, peak volume, and NOE distance calculations was carried out with Aurelia 2.7.9 (Bruker, Rheinstetten, Germany). The structure was calculated using the CNS software packet, version 1.0 (*16*), using torsion dynamics. The final set of 400 CNS-derived three-dimensional conformations were analyzed with MOLMOL (*17*), which was also used for the determination of secondary structure elements, Moleman2 and Lsqman (*18*). Rmsd values were calculated with MOLMOL and refer to average deviation of the C^α of the mean coordinates from the rest of the structures in the ensemble. An ensemble of 20 structures was selected according to lowest energy and least NOE violations. Assigned chemical shifts of *Cf* TXN1 were deposited in the BioMagResBank (http:/www.bmrb.wisc.edu/, entry number 5222); the coordinates of the structure were submitted to the Protein Data Bank (ID code 1okd).

Protein/Pseudosubstrate Interaction. ^{15}N,^{13}C-labeled TXN1 (0.05 mM) in the phosphate buffer described above was mixed with a 75 mM BOS stock solution (adjusted with NaOH to pH 6.5). During the stepwise addition of the solution to give molar ratios of pseudosubstrate to protein of 0.6, 1.4, 2.0, 2.6, and 3.8, the concentration of the protein in the NMR sample decreased by less than 3%. Two-dimensional ^1H,^{15}N HSQC NMR spectra were obtained on the Bruker Avance DMX 600 NMR spectrometer. The resolution was 1K in the ^1H dimension and 256 in the ^{15}N dimension. For each spectrum about 1000 scans were accumulated.

Molecular Modeling. Three different orientations of the pseudosubstrate to the crystal coordinates of *Cf* TXN1 suggested by NMR data were modeled with SYBYL 6.8. Coordinates for the ligand were derived from trypanothione, energy-minimized, and manually oriented on the protein surface as indicated by the NMR data. The system was then energy-minimized without any restraints using the Tripos force field. Ligand charges were calculated according to Gasteiger−Marsili. Kollmann−All charges were used for the protein. Calculations were carried out in the absence of water as molecular dynamics calculations in the presence of water tended to dissolve the protein−ligand complex. Models of a TXN−trypanothione intermediate and of the complex of reduced TXN with oxidized trypanothione were obtained accordingly for comparison purposes.

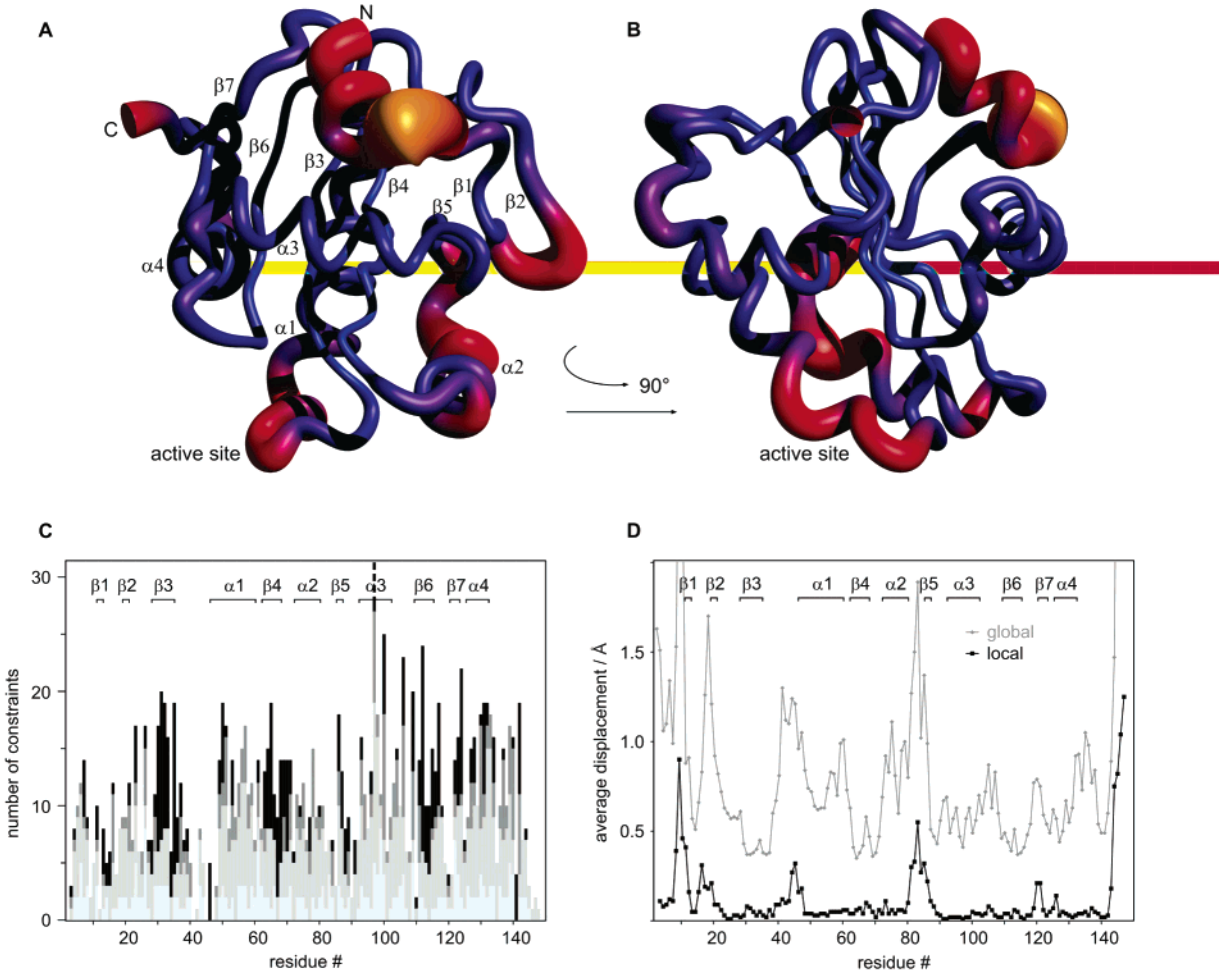

FIGURE 1: NMR analysis of *Cf* TXN1H6. (A, B) Sausage display of residues 2−144. The diameter and color (blue to orange) correspond to average displacement of structures from the mean. The most conspicuous deviations are visible for the N-terminal region, with a maximum from residue 8 to residue 11 (top), the turn between β1 and β2, helix α2 to strand β5, and the active site (bottom). The scheme was created with MOLMOL and rendered with POV-Ray (www.povray.org). (C) Number of NOE-derived distance restraints against the sequence. NOE-restraint classification according to distance separation in the primary sequence: interresidue (light gray), sequential (medium gray), medium range ($r < 5$, dark gray) and long range ($r \geq 5$, black). The scheme was created with DYANA (*26*). Note the general lack of NOE data in the "flexible" region of the active site around Cys 40 and Cys 43 and the poor long-range restraint information for residues of helix α2. In contrast, for the rigid core region comprising the strands β3, β4, β5, and β6, most of the long-range NOEs could be obtained. (D) Average global (gray, average to mean) and local (black, three sequential residues superpositioned) C^{α} displacement of the 20 calculated structures relative to the mean coordinates calculated with MOLMOL. The most noticeable features are the local displacements at the termini, at the active site (residues 40−47), and between helix α2 and strand β5.

RESULTS

Structure of Cf TXN1 in Solution. Uniformly-^{15}N,^{13}C-labeled His-tagged tryparedoxin-1 of *Cf* (*Cf* TXN1H6) afforded multidimensional NMR data that recently allowed us to determine the positions of secondary structure elements in the molecule (*19*). Here these data have been extended to provide a complete data set comprising a total of 927 NOE-derived distance restraints and 154 dihedral angles predicted with the software TALOS (*20*) (Table 1) that have been used to calculate the 3D structure. The sausage representation shown in Figure 1A,B corresponds to the 20 lowest energy conformations of 400 potential conformations calculated by CNS. The well-defined core of the protein consists of four twisted β-strands (β3, Leu 30 to Ser 36; β4, Glu 64 to Thr 69; β5, Leu 87 and Ala 88; β6, Thr 111 to Asp 116) that show a considerable number of long-range constraints (Figure 1C) and low deviations from averaged coordinates (Figure 1D). In contrast the surface-exposed β1−β2-fold, although locally well defined with rmds values of 0.52 ± 0.11 Å, is poorly defined by long-range NOE restraints, indicating flexiblity in this region of the molecule. Similar regions are found for most of helix α2, a section of helix α1 bearing the active site WCPPC motif, and those expected for the N- and C-termini.

Table 1: Parameters and Statistics for Solution Structure Calculation of *Cf* TXN1

Distance Restraints			
all	927	medium range ($\|i-j\| < 5$)	128
intraresidue	285	long range ($\|i-j\| \geq 5$)	185
sequential	329		
Dihedral Angle Restraints[a]			
all	154	Φ, Ψ	77, 77
Average rmsd of the Mean[b]			
C^{α} atoms	0.94 ± 0.12	all non-hydrogen atoms	1.46 ± 0.10

[a] Predicted with the software TALOS (*20*). [b] Rmsd in angstroms for residues Ser 2 to Phe 140 of an ensemble of 20 lowest energy structures out of 400 calculated. The rmsd values were calculated with MOLMOL and refer to the average deviation of the mean coordinates from the rest of the structure ensemble.

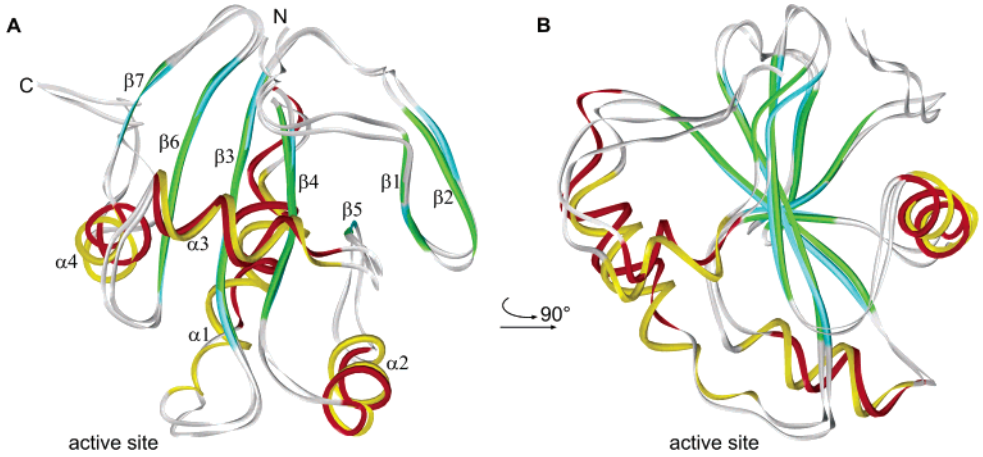

FIGURE 2: Comparison of NMR- and X-ray-derived structures of *Cf* TXN1H6. (A, B) Superposition of ribbon plots of the *Cf* TXN1 NMR mean coordinates and the crystal structure (*12*) of residues 2−148 in the same orientation as above. The secondary structure was calculated with MOLMOL [(NMR mean) red = α-helix, blue = *β*-sheet; (crystal) yellow = α-helix, green = *β*-sheet]. Slight changes in the orientation of secondary structural elements is noticeable for helices α2 and α4. Further, the amino terminal truncation of helix α1 in the solution structure (active site) is clearly visible.

Table 2: Inhibitory Activity of N^1,N^8-Bis(*γ*-Glu-Ala-Gly)spermidine toward Tryparedoxins

	[pseudosubstrate] (*μ*M)	inhibition (%) [T(SH)$_2$] = 0.72 *μ*M	[T(SH)$_2$] = 0.96 *μ*M	[T(SH)$_2$] = 1.32 *μ*M	[T(SH)$_2$] = 2.64 *μ*M	K_i (*μ*M)
Cf TXN1	400	33.8	27.4	25.0	16.2	524.9 ± 106.9
	800	54.3	45.7	47.1	35.0	
	1500	76.0	71.4	67.5	59.6	
Cf TXN2	400	26.1	26.6	25.6	21.4	791.1 ± 192.0
	800	47.0	46.2	44.5	40.2	
	1500	71.4	72.0	68.1	65.1	
Tb TXN	400		30.6			603.0 ± 97.0
	800		50.8			

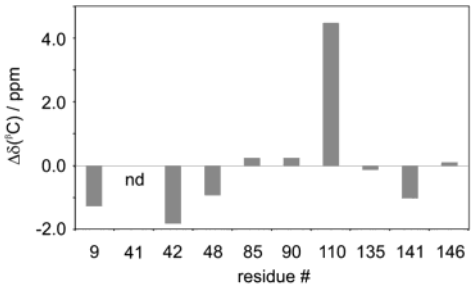

FIGURE 3: Deviation of ^{13}C chemical shifts of *β*-carbons of proline residues from the average value. nd = not determined. The abnormal low-field shift of Pro 110 (+4.5 ppm compared to the average of all prolines, +5.1 ppm compared to the average of all prolines except Pro 110) indicated a *cis* peptide bond (*27*).

The general folding pattern and core structure elucidated here for *Cf* TXN1H6 in solution are identical (Figure 2) with those found in the crystal structure (*12*). The flexibility found here for α2 relative to *β*4 (Figure 1) is compatible with the discrete locational differences of up to 1.8 Å for this region of the molecule in TXN X-ray structures (*12*, *21*) and suggest this may be of functional importance. In addition the chemical shift behavior of the proline *β*-carbons (Figure 3) indicates that in solution only the Ile 109−Pro 110 exists in a *cis* configuration. A second *cis* peptide bond for Pro 141 found in all crystal structures (*12*, *21*) is predominantly *trans* in solution. This is perhaps not unexpected as previous data for small linear peptides in solution indicate that, although the *cis* content of sequencially similar peptides is unusually high, the *trans* configuration predominates (*22*).

Inhibition of Cf TXNs by N^1,N^8-Bis(ophthalmyl)spermidine. The redox-inactive homologue of trypanothione BOS weakly inhibited the two TXN isozymes of *Cf* and TXN of *Tb* (Table 2), and showed competitive inhibition toward trypanothione (data not shown). Inhibition constants calculated on this basis were in the high micromolar range, as expected from the weak TXN/trypanothione interaction presumed to primarily depend on electrostatic attractions of the (pseudo)substrate's carboxylic functions and arginine residues at the enzyme surface (*12*). Interestingly, the bis(ophthalmyl) derivative of diaminooctane did not inhibit TXN up to a concentration of 2 mM, indicating that the secondary amino group of the spermidine moiety in trypanothione contributes to substrate binding.

Pseudosubstrate-Induced Chemical Shifts. Titration of ^{15}N,^{13}C-*Cf* TXN1H6 with the unlabeled pseudosubstrate BOS (Figure 4) caused considerable shifts of about 20% of the protein's NH resonances in 2D ^{1}H,^{15}N HSQC spectra (Figure 5). The original resonance usually remained detectable up to a 2.6-fold molar BOS excess. Gradually increasing the BOS concentration caused the intensity of "new" resonances to increase at the expense of the original ones, thereby facilitating assignment of the residues affected by BOS binding.

As expected, the shifted resonances could be assigned to residues of the active-site motif 39 WCPPCR 44 (Trp 39, Cys 40, Cys 43, Arg 44) or to those implicated in substrate binding such as Glu 72 and Ile 109 (*12*). Nearly all shifts could be assigned to surface-exposed residues, but a con-

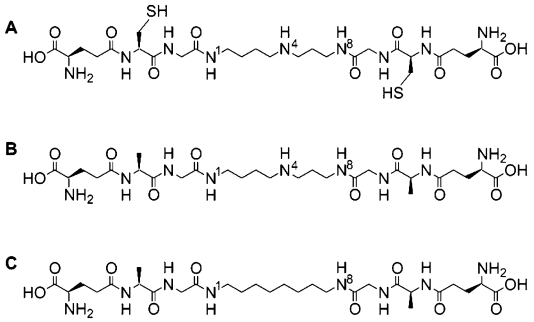

FIGURE 4: Structures of trypanothione (N^1,N^8-bis(glutathionyl)-spermidine, reduced form (A), and the redox-inactive derivatives N^1,N^8-bis(γ-Glu-Ala-Gly)spermidine (BOS) (B) and N^1,N^8-bis(γ-Glu-Ala-Gly)diaminooctane (C).

siderable proportion to sites that are considered to be irrelevant to catalysis. Figure 6 shows that the residues affected by BOS cluster near the active site yet spread almost over the entire "front side" surface and even to the back of the protein (Figure 6B). Since these observations may indicate unspecific interactions of BOS with the TXN superimposed on specific ones, the possibilities of binding were explored by docking the flexible pseudosubstrate to the protein.

In Silicio Generation of Putative Complexes. Docking of BOS to *Cf* TXN1 by automated standard programs such as Autodock proved to be unproductive. This approach yielded a bewildering variety of proposals, most of them reminiscent of little else than stochastic attractions of inversely charged residues. To reduce the number of binding options to those potentially relevant to TXN activity and inhibition thereof, we took advantage of the model of $T(SH)_2$/TXN interaction deduced from X-ray data and site-directed mutagenesis (*12*). It presumes that binding of $T(SH)_2$ to TXN starts with electrostatic binding between the carboxylic group of the N^1-bound glutathione to Arg 128 of TXN that is strengthened by hydrogen bridges to the *cis* Ile 109−Pro 110 bond and directs the substrate's thiol group into a strategic position to react with the disulfide bridge between Cys 40 and Cys 43 of the TXN. Termination of the catalytic cycle, i.e., formation of the cyclic disulfide form of trypanothione, requires that the N^8-bound glutathione is bent toward the redox center.

If an identical starting position is assumed for the initial binding of the homologous BOS, as is demonstrated in Figure 7 A, essentially three possibilities of BOS orientation are proposed by energy minimization: The second carboxylic group of BOS projects toward Arg 15 (Figure 7B), interacts with a basic area composed of Lys 6, Lys 99, Lys 102, and His 103 (Figure 7D), or is attracted by Lys 83 and Arg 44 (Figure 7C). Out of these proposed binding modes only the one shown in Figure 7C comes close to an enzyme−substrate complex that can be envisaged to be productive, as is discussed below and demonstrated in Figure 8. In contrast the models shown in Figure 7B,D mimic unproductive complexes, since here the N^8-bound ophthalmyl residue, which substitutes for the glutathionyl residue of $T(SH)_2$, is oriented away from the reaction center. All these binding modes nevertheless appear to be realistic as in toto they account precisely for the surface area of the enzyme's front side (Figure 6A), which shows chemical shift changes. From the few backside residues responding to BOS (Figure 6B) Arg 16 may be indirectly affected by the neighboring Arg 15, which implies that the remaining 3−4 contiguous residues may indicate BOS binding modes beyond the ones depicted in Figure 7. Comparison of binding models and pseudosubstrate-induced chemical shifts thus reveal that the highly flexible ligand can indeed be bound to TXN in different orientations, which are homologous to productive enzyme−substrate complexes, transient catalytic conformations, or inhibitory binding modes.

DISCUSSION

The structure of *Cf* TXNH61 in solution here elucidated by NMR techniques for the first time essentially complies with the X-ray-based structures of *Cf* TXN1 (*12*, *21*), *Cf* TXN1H6 (*12*), *Cf* TXN2H6 (*12*), and *Cf* TXN2H6C44S (*12*). The congruence of the folding pattern and, in particular, of the four twisted β-strands, which make up most of the protein core, underscores the rigidity of the thioredoxin fold which is shared by the TXNs. The NMR structure of *Cf* TXN1H6 remains less defined at the C- and N-termini, near the active site, in the $\beta1-\beta2$ turn and in the $\alpha2$ helix, which is absent in the thioredoxins. In particular, the structural ambiguity of the $\alpha2$ helix may reflect physical flexibility, since discrete differences of its location were also detected between the different X-ray structures. More importantly, the 2D spectra enabled us to study the molecular contacts with a closely related homologue of the substrate and thus deepened our understanding of how TXN may handle its specific substrate $T(SH)_2$.

Kinetic analyses with different TXNs have consistently disclosed a "ping-pong mechanism" or "enzyme-substitution mechanism": The TXN is reduced by $T(SH)_2$, and the product TS_2 has to leave the reduced TXN before the latter can interact with its downstream proteinaceous substrate TXNPx (*5*, *15*). Accordingly, any attempt to cocrystallize a TXN with $T(SH)_2$ failed (*12*). Crystals were only obtained of a dead-end intermediate formed by reacting the inactive mutant *Cf* TXN2H6C44S with the pseudosubstrate glutathionylspermidine. Therein, the pseudosubstrate's glutathionyl sulfur was bound to the surface-exposed Cys 41 thiol of TXN2, its carboxylic group formed an ideal salt bridge to Arg 129, and the cysteyl moiety sustained hydrogen bridges with the *cis* Ile 110−Pro 111 bond (position numbers in *Cf* TXN1 differ by 1 from those in *Cf* TXN2). On the basis of these crystallographic data, a model of the TXN/$T(SH)_2$ interaction was developed that, however, had to rest on site-directed mutagenesis data and modeling-supported plausibility consideration, as far as binding of the remaining parts of the substrate is concerned. This dynamic model considers the N^1-glutathionyl binding, as seen in the crystallized dead-end intermediate, to initiate the process and to trigger the reaction of the first substrate's SH with Cys 41 and binding of its secondary amino group to Glu 72. This facilitates the transition to a productive conformation which is finally achieved by binding of the N^8-glutathionyl to Arg 45, whereupon TXN is reduced by the N^8-glutathionyl SH (*12*).

The shifts of the NH resonances induced by BOS indicate the residues of TXN that are involved in ligand binding, although such chemical shift pertubations do not allow any reliable quantitative calculation of interaction energies and may fail to precisely locate ligands at protein surfaces (*23*). More detailed information would be provided by intermo-

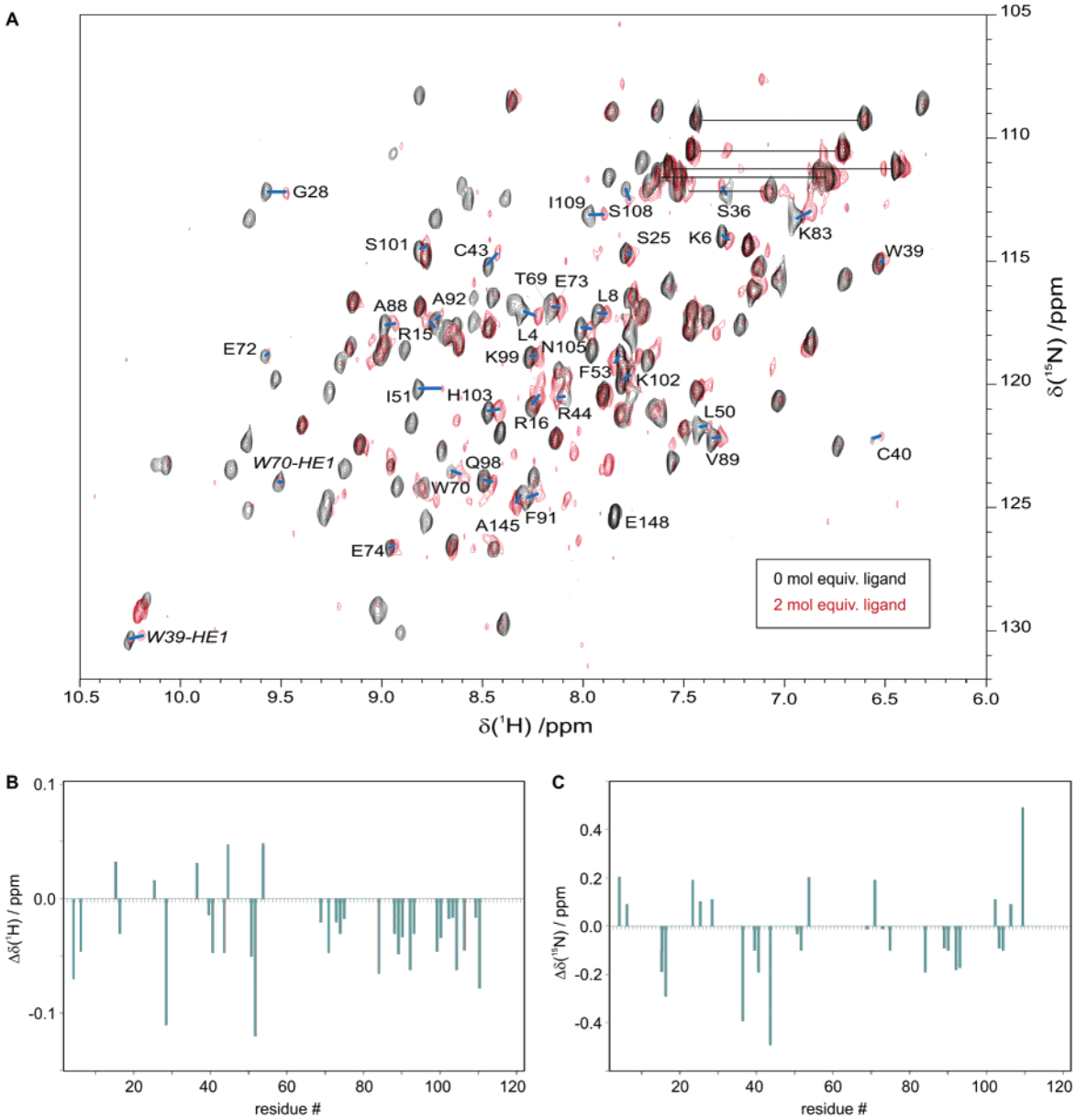

FIGURE 5: Resonance shifts induced by binding of pseudosubstrate. (A) Region of overlayed 2D $^{1}H,^{15}N$ NMR spectra documenting the signal shift of TXN upon addition of the pseudosubstrate BOS: black without BOS; red with two molar equivalents of the compound. Signals of residues near the active site, which were identified to definitely exhibit chemical shifts during addition of ligand, are indicated with blue bars and marked with the corresponding residue ID. The signal shift of the amide NH resonances of Ile 109 and Cys 43 and the aromatic side chain NH of Trp 39 are clearly visible. The horizontal black bars indicate NH signals of asparagine and glutamine side chains. Unassigned weak red cross-peaks arise from degradation products that accumulate toward the end of the titration series. (B) Significant shift deviations of the amide proton and (C) ^{15}N resonances of residues 2−120 determined in the absence and presence of two molar equivalents of ligand. Only resonances with proton shifts above 0.01 ppm were considered.

lecular NOEs, which, however, are hard to detect with low-affinity ligands. An alternative method using simulation of proton chemical shift pertubations may precisely localize low-affinity ligands but depends on the aromatic nature of the ligand (*23*), which does not apply to $T(SH)_2$ or BOS. Despite their limitations, our conventional analyses of $^{1}H-^{15}N$ chemical shifts (Figures 5 and 6) strongly support our model of the TXN/(pseudo)substrate interaction. BOS binding, as shown in Figure 7C, comes very close to a productive-like conformation of the catalytic intermediate and shows all the implicated homologous residues of TXN1 involved in BOS binding: Arg 128, Cys 40, Ile 109, Pro 110, Glu 72, and Arg 44. Out of these only Arg 128 does not respond to BOS with a chemical shift in the 2D spectrum, presumably because structural changes are restricted to the side chain and alterations at the backbone NH are too small. While the involvement of Arg 128, Cys 40, Ile 109, and Pro 110 in the catalysis has already been evident from X-ray data (*12*), the contribution of Glu 72 and Arg 44 to substrate binding is shown here experimentally by pseudosubstrate-induced shift pertubations.

Replacing BOS by $T(SH)_2$ in the "productive intermediate conformation" (Figure 8) underscores the dynamic nature of the process: In Figure 8A the N^{1}-bound glutathionyl residue is bound to Arg 128 and the Ile−Pro bond, as seen in the crystallized dead-end intermediate, and the basic spermidine nitrogen is attracted by Glu 72, as inferred from site-directed mutagenesis data. In Figure 8B the catalytic

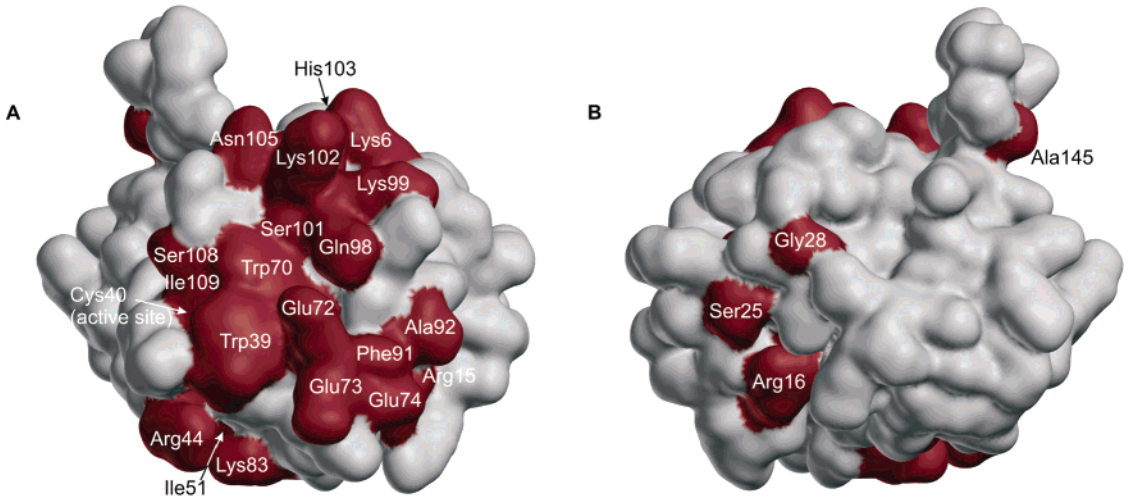

FIGURE 6: Surface model of *Cf* TXN1. Surface-exposed residues, which exhibit shifts of amide HN resonances [(^{1}H) ≥0.01 ppm and/or (^{15}N) ≥0.02 ppm) in the 2D ^{1}H,^{15}N NMR experiment during addition of pseudosubstrate, are labeled in brown. (A) "Front" view of the protein, showing the active site and contiguous residues in three regions that interact with the ligand. (B) At the "backside" only a few residues exhibit signal shifts. Those of Gly 28, Ser 25, and Ala 145 probably resulted from unspecific interactions. Arg 16 marks the surface-exposed guanidino function of this residue. The resonances of its amide group, which is buried in the $\beta1-\beta2$-loop, could be influenced by Arg 15, which is presumed to be directly involved in ligand binding.

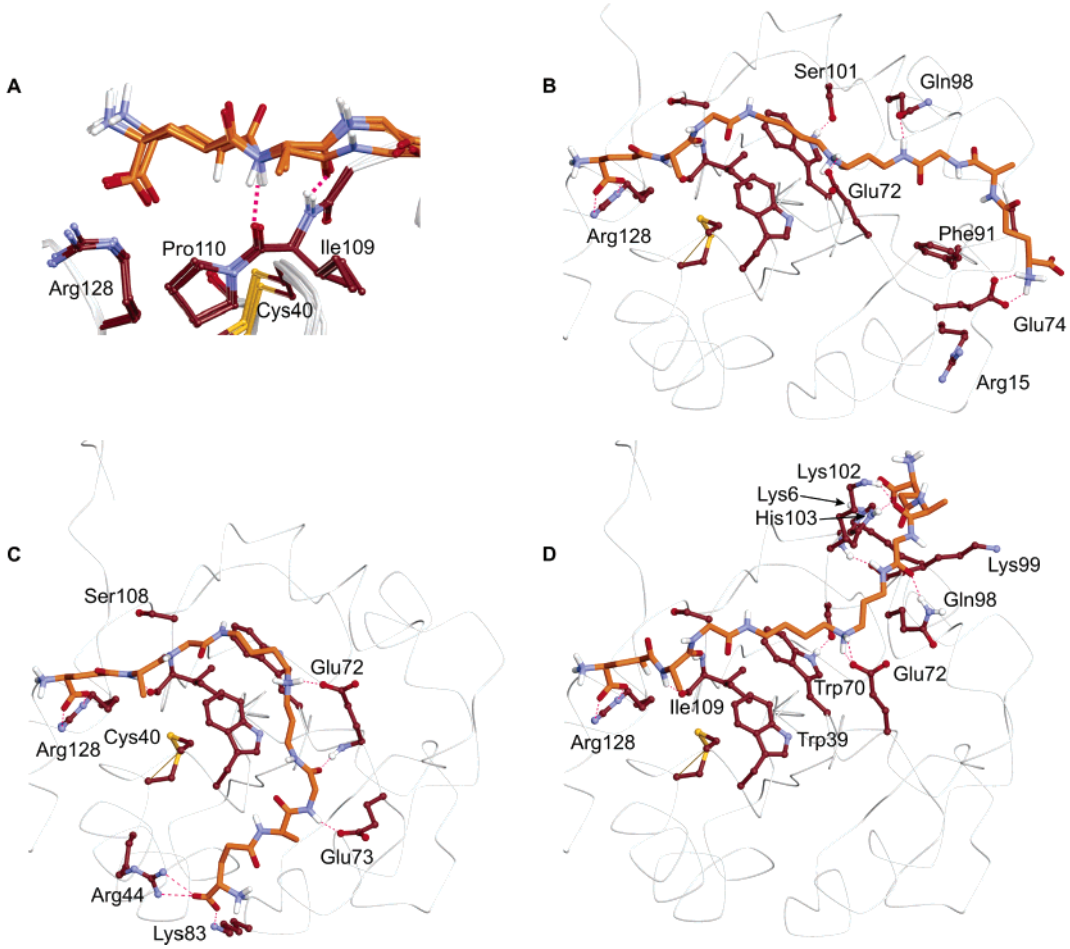

FIGURE 7: Variability of the TXN/BOS interaction. Models of the pseudosubstrate docked to *Cf* TXN1. (A) Presumed interaction of the active site of TXN with the N^1 moiety of the pseudosubstrate (orange stick model). The N^1-carboxylic group of the pseudosubstrate is electrostatically bound to the guanidino function of Arg 128. H-bonds between Ile 109 and the ligand are symbolized with pink dotted lines. (B−D) Energy-minimized models of the docked pseudosubstrate. Residues with NMR signal shifts (except Arg 128) are displayed as brown stick models. In line with NMR data, the N^8-carboxyl function of the pseudosubstrate can electrostatically be bound to Arg 15, Arg 44, or His 103.

intermediate has been formed, the spermidine nitrogen is slightly turned away from the Glu 72 carboxylic group, and the N^8-bound glutathione becomes attracted by Arg 44, whereby its thiol group migrates into a strategic position to attack the disulfide bond of the catalytic intermediate. To cyclize into its disulfide form, trypanothione has to loosen

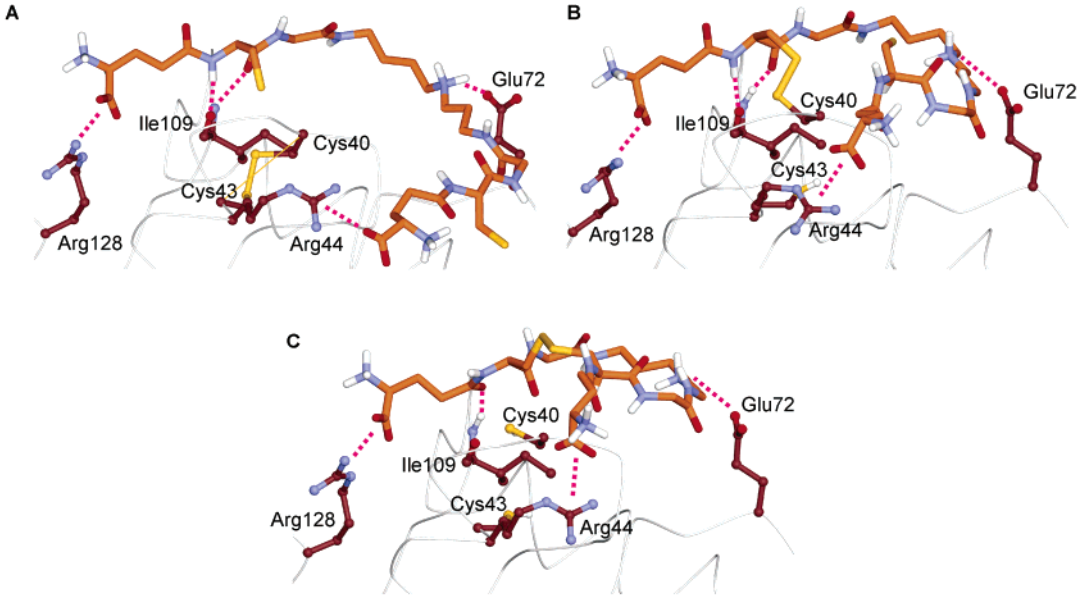

FIGURE 8: Models of oxidized and reduced *Cf* TXN1 with trypanothione. (A) Oxidized TXN with bound trypanothione, structurally analogous to the pseudosubstrate model in Figure 7C with the H-bonds to Ile 109 still existent. The N^8-terminal carboxylic function is coordinated to Arg 44. (B) Comparable model with the trypanothione disulfide bound to Cys 40. The free thiol function of trypanothione is oriented to the active site. (C) Reduced TXN with coordinated oxidized trypanothione. Compared with the noncyclic form, the H-bonding to Ile 109 is weakened and the attachment to the protein is decreased.

most of its contacts with the enzyme (Figure 8C). In particular, the hydrogen bridges to the *cis* Ile 109−Pro 110 bond are weakened, and the remaining salt bridges to Arg 44 and Arg 128 are not strong enough to keep the product attached.

The conformations of the pseudosubstrate BOS, shown in Figure 7B,D, cannot be reconciled with any productive complex or intermediate of the true catalytic process. This does, however, not imply that these modes of binding are functionally irrelevant. Oriented as in Figure 7B,D, the substrate might still have a chance to switch toward the more productive orientation shown in Figure 7C for the pseudosubstrate or Figure 8A for the true substrate. But, in essence, the modes of substrate binding depicted in Figure 7B,D are unproductive. Thus, if Arg 44 in the α_1 helix is occupied by another carboxylic group of excess substrate, they would be inhibitory. The set of NMR data reveal that such unproductive pseudosubstrate binding to the basic cluster composed of Lys 6, Lys 99, Lys 102, and His 103 or to Arg 15 does indeed occur. This finding provides an explanation for the pronounced inhibition of TXN by high concentrations of its physiological substrate $T(SH)_2$ (*24*). The inappropriately bound substrate molecules impair the formation of productive complexes. They also prevent binding of the bulky proteinaceous cosubstrate TXNPx that most likely depends on the same residues as those of $T(SH)_2$ binding, i.e., Arg 128, Arg 44, and acid residues of helix α_2 (*9*). In the normal catalytic cycle, $T(SH)_2$ is bound, processed, and released as product to allow access of the cosubstrate to the reaction center, a sequence of events characterizing a ping-pong mechanism that has been demonstrated by steady-state kinetics (*25*). Excess $T(SH)_2$ bound unproductively would, however, have to be competitively removed by cosubstrate. This was indeed observed in the kinetic analysis of *Cf* TXN2 where the inhibition by excess $T(SH)_2$ could be overcome by increasing concentrations of *Cf* TXNPx (*24*). In short, the multiple possibilites of (pseudo)substrate binding by TXN here documented by chemical shift changes upon titration with pseudosubstrate explain both the basic catalytic mechanism and the cosubstrate-compensated substrate inhibition.

The ultimate goal, which is the design of therapeutically useful inhibitors of TXNs, is evidently not met by flexible peptides mimicking the substrate. The inhibition constant of BOS was weak, BOS was easily competitively removed by the real substrate, and BOS binding could reliably be characterized by NMR in the absence of substrate only. The study nevertheless discloses which parts of the TXN surface are functionally relevant, and this sets the frame to design more rigid and active ligands. The comparatively unstructured substrate interaction site of the TXNs, however, will remain a serious hurdle to create strong reversibly binding ligands. The solution of this problem might consist in the use of irreversible thiol modifiers which, by taking advantage of the knowledge of possible substrate binding modes, are to be designed to specifically attack the surface-exposed thiol (Cys 40 or Cys 41) of the TXNs.

ACKNOWLEDGMENT

We thank Dr. Wolfram Gronwald, Institut für Biophysik und Physikalische Biochemie, Universität Regensburg, for kind support and helpful discussions.

REFERENCES

1. Seed, J. R. (2001) *Int. J. Parasitol. 31*, 434−442.
2. Schofield, C. J., and Maudlin, I. (2001) *Int. J. Parasitol. 31*, 615−620.
3. Anene, B. M., Onah, D. N., and Nawa, Y. (2001) *Vet. Parasitol.* 96, 83−100.
4. Matovu, E., Seebeck, T., Enyaru, J. C. K., and Kaminsky, R. (2001) *Microb. Infect. 3*, 763−770.
5. Nogoceke, E., Gommel, D. U., Kiess, M., Kalisz, H. M., and Flohé, L. (1997) *Biol. Chem. 378*, 827−836.
6. Tovar, J., Wilkinson, S., Mottram, J. C., and Fairlamb, A. H. (1998) *Mol. Microbiol.* 29, 653−660.

7. Krieger, S., Schwarz, W., Ariyanayagam, M. R., Fairlamb, A. H., Krauth-Siegel, R. L., and Clayton, C. (2000) *Mol. Microbiol. 35*, 542−552.
8. Flohé, L., Hecht, H. J., and Steinert, P. (1999) *Free Radical Biol. Med. 27*, 966−984.
9. Hofmann, B., Hecht, H. J., and Flohé, L. (2002) *Biol. Chem. 383*, 347−364
10. Wood, Z. A., Schröder, E., Harris, J. R., and Poole, L. B. (2003) *Trends Biochem. Sci. 28*, 32−40.
11. Fairlamb, A. H., Blackburn, P., Ulrich, P., Chait, B. T., and Cerami, A. (1985) *Mol. Biochem. Parasitol. 14*, 187−98.
12. Hofmann, B., Budde, H., Bruns, K., Guerrero, S. A., Kalisz, H. M., Menge, U., Montemartini, M., Nogoceke, E., Steinert, P., Wissing, J. B., Flohé, L., and Hecht, H.-J. (2001) *Biol. Chem. 382*, 459−471.
13. Guerrero, S. A., Flohé, L., Kalisz, H. M., Montemartini, M., Nogoceke, E., Hecht, H.-J., Steinert, P., and Singh, M. (1999) *Eur. J. Biochem. 259*, 789−794.
14. McKay, F. C., and Albertson, N. F. (1957) *J. Am. Chem. Soc. 79*, 4686−4690.
15. Flohé, L., Steinert, P., Hecht, H. J., and Hofmann, B. (2002) *Methods Enzymol. 347*, 244−258.
16. Brünger, A. T., Adams, P. D., Clore, G. M., Delano, W. L., Gros, P., Grosse-Kunstleve, R. W., Jiang, J.-S., Kuszewski, J., Nilges, M., Pannu, N. S., Read, R. J., Rice, L. M., Simonson, T., and Warren, G. L. (1998) *Acta Crystallogr. D54*, 905−921.
17. Koradi, R., Billeter, M., and Wüthrich, K. (1996) *J. Mol. Graphics 14*, 51−55.
18. Kleywegt, G. J. (1999) *Acta Crystallogr. D55*, 1878−1884.
19. Krumme, D., Hecht, H.-J., Menge, U., Ross, A., Wray, V., and Flohé, L. (2002) *J. Biomol. NMR 21*, 375−376.
20. Cornilescu, G., Delagio, F., and Bax, A. (1999) *J. Biomol. NMR 13*, 289−302.
21. Alphey, M. S., Leonard, G. A., Gourley, D. G., Tetaud, E., Fairlamb, A. H., and Hunter, W. N. (1999) *J. Biol. Chem. 274*, 25613−25622.
22. Grathwohl, C., and Wüthrich, K. (1976) *Biopolymers 15*, 2025−2041.
23. McCoy, M. A., and Wyss, D. F. (2000) *J. Biomol. NMR 18*, 189−198
24. Steinert, P., Plank-Schumacher, K., Montemartini, M., Hecht, H.-J., and Flohé, L. (2000) *Biol. Chem. 381*, 211−219.
25. Gommel, D. U., Nogoceke, E., Morr, M., Kiess, M., Kalisz, H. M., and Flohé, L. (1997) *Eur. J. Biochem. 248*, 913−918.
26. Güntert, P., Mumenthaler, C., and Wüthrich, K. (1997) *J. Mol. Biol. 273*, 283−298.
27. Wüthrich, K. (1976) *NMR in Biological Research: Peptides and Proteins*, North-Holland Publishing Co., Oxford.

BI030112D